Journal of Power Sources 224 (2013) 250–259

Contents lists available at SciVerse ScienceDirect

Journal of Power Sources

journal homepage: www.elsevier.com/locate/jpowsour

Dip–spin coating of reticulated vitreous carbon with composite materials to act as an electrode for 3D microstructured lithium ion batteries

Matthew Roberts*,[1], An Feng Huang, Phil Johns, John Owen

School of Chemistry, University of Southampton, Southampton, Hampshire SO172LU, United Kingdom

HIGHLIGHTS

- A technique for coating 3D substrates in layers of composite electrode material is presented.
- Uniform layers containing $LiFePO_4$, $LiMn_2O_4$ and TiO_2 have been deposited on carbon foams.
- Samples with a high area specific capacities (>1000 μA h cm^{-2}) have been prepared.
- High rate performance (~50% DOD at 25 C) was also observed for the same sample.

GRAPHICAL ABSTRACT

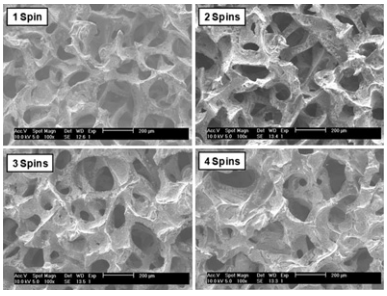

ARTICLE INFO

Article history:
Received 18 May 2012
Received in revised form
15 August 2012
Accepted 30 September 2012
Available online 8 October 2012

Keywords:
Dip–spin coating microbattery
$LiFePO_4$
Reticulated vitreous carbon
$LiMn_2O_4$
TiO_2

ABSTRACT

This paper describes a new and economic route for the formation of three dimensional (3D) microstructured battery electrodes using our "in house" developed dip–spin coating technique for depositing layers of active material onto reticulated vitreous carbon (RVC) substrates. These coatings are optimized composite materials containing carbon black and polymer binder to facilitate good electronic and ionic conductivities through the electrode. The application process begins by immersing the substrate in an ink followed by rapid spinning to provide a uniform coating with a well controlled mass loading. The performance of the electrodes was investigated in lithium ion cells as a function of the composition of the inks used and the number of dip–spin coating cycles.

Optimization of the ink composition, dip and spin parameters has improved the electrochemical performances of the electrodes to give state of the art footprint area specific capacities (>1000 μA h cm^{-2}) and high rate capabilities (nearly 50% degree of discharge at 25 C) in lithium half cells. This represents the first stage in the development of a full 3D microbattery system. Initial results have also shown the versatility of this approach in depositing other electrode materials by forming uniform layers of both TiO_2 and $LiMn_2O_4$.

1. Introduction

As the size of the electronics in many of today's portable devices becomes smaller and more sophisticated the limiting factor, in terms of device size and power consumption, is more often than not the battery. Accordingly, advances in microelectromechanical systems (MEMS), miniaturized medical implants and on chip power supplies have driven the development of a new generation of batteries termed "3D microbatteries" that have been the focus of many recent publications [1–7]. The 3D microbattery concept combines the use of a thin film cathode, electrolyte and anode with a high surface area three dimensional substrate [1,8,9] to create a battery with a total size that is typically less than few cubic

* Corresponding author. Tel./fax: +44 (0) 2380 59 4114.
E-mail address: mrr100@soton.ac.uk (M. Roberts).
[1] Also at Department of Materials Chemistry, Uppsala University, Box 538, SE 75121, Uppsala, Sweden.

0378-7753/$ – see front matter © 2012 Elsevier B.V. All rights reserved.
http://dx.doi.org/10.1016/j.jpowsour.2012.09.103

millimeters. The aim of this work is to utilize the high rate performance that can be achieved with thin film batteries [10] whilst improving the capacity per footprint area by depositing thin electrode films on high surface area 3D substrates.

There are numerous publications detailing methods of cathode material deposition. Golodnitsky et al. have electrodeposited molybdenum sulfide films onto gold coated perforated silicon plate substrates to form 3D cathodes for lithium ion insertion [11]. More recently the same group developed their technique to make use of CuS [12] cathodes whilst also electrophoretically depositing $LiFePO_4$ [13] onto the perforated silicon substrates. Both examples demonstrated a significant increase in capacity per footprint area compared with a planar electrode. Another example is the work of Min et al. [5] who used an array of carbon pillars as the 3D substrate. Alternating pillars were then coated in polypyrrole (used as the positive electrode), leaving the remaining carbon pillars to act as the negative electrode. This fabrication method produced high quality electrode arrays with an impressively short interelectrode spacing giving a potential for very high rate performance; however, results indicated problems due to electrical short circuits within the arrays and rate limitations due to the large resistances associated with the carbon pillars.

Our recent publication on the use of MnO_2 (sometimes referred to a Electrolytic Manganese Dioxide (EMD)) as a 3D cathode material clearly showed the enhancement of capacity per footprint area that can be achieved when coatings are applied to reticulated vitreous carbon (RVC) substrates [14]. This publication carefully characterized vitreous carbon substrates with high pore densities which gave surface areas of up to 30 times the geometric area for a foam thickness of 1 mm. Such materials also have the advantage of having enough porosity to accommodate the cathode, electrolyte, anode and current collector layers necessary for a full 3D battery system. The rate performance was correspondingly improved, although the discharge rate was ultimately limited by slow diffusion in the rather dense and compact electrodeposited MnO_2 material (this is a serious drawback with electrochemically deposited layers where it is difficult to tune the porosity to achieve good lithium ion diffusion through the layer where no conductive additive is included to enhance electronic conductivity). This limitation is particularly severe in cases where thicker electrodes (2–5 μm) are required to give high specific energies in macroporous structures. Another problem with electrodeposition is its limited range of applicability in the field of battery materials, where MnO_2 is a rather uncommon example of a material that can be deposited easily. Therefore a new approach is needed to widen the choice of electrode materials and thus further improve footprint capacities and rate performance.

In this work we have adopted a new method to deposit layers of a *composite* electrode containing nanoparticulate active material, binder and conductive additive on the surface of reticulated vitreous carbon foams (RVC) to form a hierarchically porous structure. The basic principle is similar to the spin coating method commonly used for coating planar substrates used in photo resist technologies. Specifically the approach is applied to a three-dimensional surface by dipping the RVC substrate into an ink (to infiltrate the sample with active materials, conductive additive and binder) before removing and spinning to eject excess ink and rapidly dry any remaining solvent. This process results in a portion of the solid fraction of the ink being deposited on the struts of the RVC substrate, and surprisingly produces a relatively uniform thick film in the same way as in the analogous spin coating method used to coat planar substrates, we refer to the method as "dip–spin coating". The combination of relatively cheap cathode materials and inexpensive three dimensional RVC substrate is envisaged as an attractive and economic route to produce 3D microbatteries.

Three different electrode materials are used to demonstrate the versatility of the 3D spin coating process. The majority of the work focuses on $LiFePO_4$, which is of great interest as a safe and environmentally acceptable positive electrode for lithium ion batteries [15,16]. Nanoparticulate $LiFePO_4$ was chosen for this study due to its small particle size, allowing it to be easily suspended within an ink without rapid sedimentation. Optimized forms of this material with conductivity-enhancing surface coatings of pyrolytic carbon are now providing low cost alternatives to $LiCoO_2$, exhibiting relatively high capacities of up to 168 mA h g^{-1} at 3.45 V vs. lithium. Another competitive alternative lithium ion cathode material is the spinel form of $LiMn_2O_4$ which cycles at a higher voltage, between 4.2 and 3.7 V vs. Li albeit a lower capacity of around 115 mA h g^{-1} due to a narrower range of phase stability during cycling [17–19]. Finally, nanoparticulate TiO_2 of the anatase structure with a typical capacity [20,21] of 200 mA h g^{-1} was deposited on 3D RVC to form an example of a negative electrode. Despite its rather high potential for lithium insertion, between 1.7 and 1.3 V vs. Li, this material was considered most suitable for the 3D negative electrode because it avoided complications due to irreversible reactions and Li insertion into carbons commonly encountered below 1 V vs. Li.

The aims of this work were as follows:

- To develop a generic method for conformally coating composite electrode materials onto the entire internal surface area of 3D reticulated vitreous carbon foams.
- To characterize the performance of the dip–spin coated composite/RVC foam electrodes as half cells vs. Lithium.

2. Experimental section

2.1. Materials

The reticulated vitreous carbon (compressed 100 ppi (pores per inch)) (shown in Fig. 3) was purchased from ERG materials and aerospace engineering. This foam gives an area enhancement of approximately 30 times per geometric area for a piece of foam 1 mm thick (The details about the area gain of these materials have been reported in previous publications [14]). The strut size is approximately 40 μm thick and the window size (which is the hole linking between the different cells making the foam like structure) is approximately 100 μm in diameter as seen in Fig. 3. The porosity of the foam is approximately 75%. The density of the foam as purchased is approximately 0.4 g cm^{-3}. The $LiFePO_4$ with a carbon coating was kindly provided by Dr Karim Zaghib of Hydroquebec. The $LiMn_2O_4$ was supplied by Carus Chemical. The acetylene black (Shawinigan Black, 100%-compressed) was supplied by Chevron Phillips Chemical company. The TiO_2 (99.5% anatase) nanoparticles, PVdF-HFP, CP and Li metal were all supplied by Aldrich. The electrolyte was 1 M $LiPF_6$ in 1:1 EC/DMC provided by Purelyte.

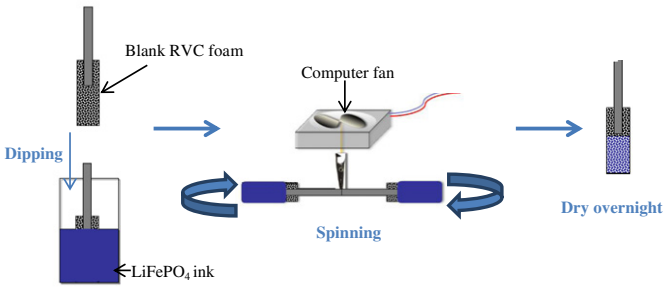

Fig. 1. The full process of dip coating followed by rapid spin drying; "dip–spin coating".

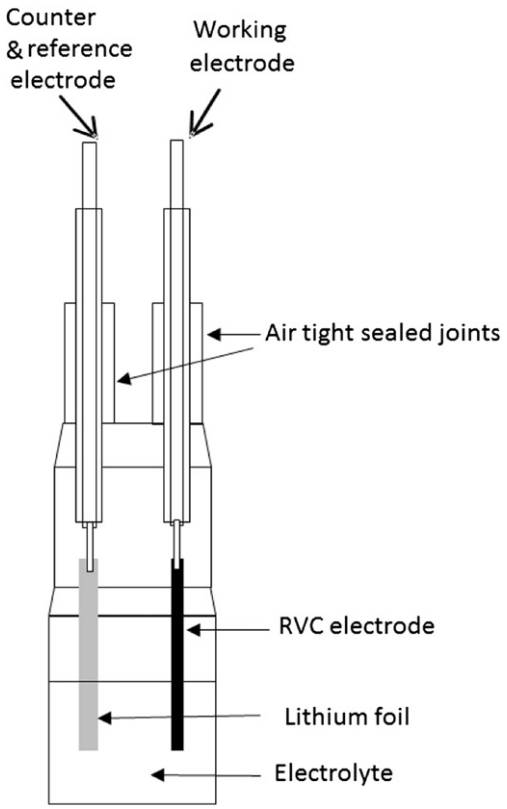

Fig. 2. A schematic diagram of the assembled two-electrode cell in a electrolyte bath.

2.2. Ink preparation

Inks were prepared in different solid weight percentages. If an ink is said to be 10 wt. % then 100 g of ink contains 10 g of solid component. These solids included the active material which was of three types: first $LiFePO_4$ (60%), Acetylene Black (AB) (30%) and PVdF-HfP (10%) binder, second $LiMn_2O_4$ (60%), AB (30%) and PVdF-HfP (10%) binder and third TiO_2 (60%), AB (30%) and PVdF-HfP (10%) binder. A relatively large amount of acetylene black was used to ensure good electronic conductivity in this proof of concept study. The inks were prepared by mixing the solid components in cyclopentanone, the mixture was stirred for around 10 h at room temperature to ensure the formation of a homogeneous ink.

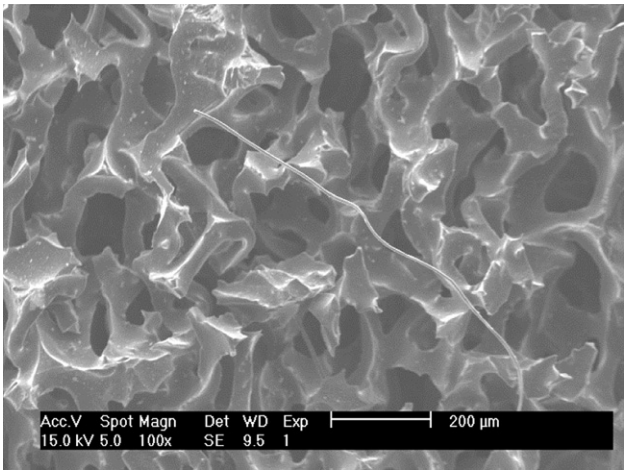

Fig. 3. SEM image of 100 ppi compressed reticulated vitreous carbon substrates used in this work. As an indication of scale a single 7 µm thick carbon fiber is included in this image on top of the foam.

2.3. Dip coating followed by rapid spin drying technique (or "dip–spin coating")

Conventional techniques for the spin coating of substrates have existed for many years and the literature is replete with examples of this process. The dip–spin coating apparatus was kept as simple and low cost as possible (a schematic of the preparation method is shown in Fig. 1): a 10 V computer fan was mounted in a Perspex box. A crocodile clip was then attached perpendicular to the center of the fan using a quick setting epoxy. The carbon foam substrates were then prepared by attaching a small titanium foil tab to the foam using a quick set epoxy resin (RS components). The foams were then dipped into the ink for a few seconds to allow penetration into the structure, the resulting capillary action drawing the inks into the foam. The Ti tab was then secured in the crocodile clip. The dip–spin coating apparatus was driven by applying a voltage to the fan, the rotation rate was measured as being between 2000 and 3000 rotations per minute (rpm). The rotation was applied for 30 s and the sample removed, further dipping and spinning steps were applied if a higher degree of active material loading was required.

2.4. SEM characterization

Scanning electron microscopy (SEM) was used to characterize the materials using a Philips XL30 Environmental SEM and the secondary electron detectors. A sharp scalpel was used to cut through and image the cross-section of the $LiFePO_4$|RVC electrodes (Fig. 3).

2.5. Thermogravimetric analysis (TGA)

Using a TA Instruments TGA Q500 thermogravimetric analysis system TGA traces were recorded. This was measured between room temperature and 600 °C at a heating rate of 1 °C min^{-1}.

2.6. Electrochemical characterization

The $LiFePO_4$|RVC electrodes were characterized in liquid electrolyte vs. a Li metal counter (Fig. 2). Connection to the RVC was made via a pressure contact applied by a stainless steel screw as shown in Fig. 2. The test cell was constructed under argon <0.1 ppm O_2 and H_2O. The various $LiFePO_4$|RVC electrodes were cycled galvanostatically between 4.2 and 2 V vs. Li/Li^+. All electrochemical testing was done using a Variable Multichannel Poteniostat 2 (VMP 2) (Bio-logic). C rates were difficult to calculate because the exact amount of active material deposited onto the foam was difficult to ascertain. Therefore a 2 h discharge was used to acquire the nominal capacity of the cell and C rates were then calculated based on this capacity.

2.7. Electrochemical testing of conventional electrodes

Electrode film pellets containing 75 weight % (wt. %) of $LiFePO_4$, 20 wt. % of acetylene black (Shawinigan Black, 100%-compressed, Chevron AB), and 5 wt. % poly(tetrafluoroethylene) (PTFE, Type: 6C–N, DuPont) binder were prepared as described previously [10]. Two-electrode cells were assembled in an argon filled glovebox (H_2O, O_2 < 1 ppm; Unilab from MBraun). Lithium foil was used as both the counter and the reference electrode, and 1 M $LiPF_6$ in ethylene carbonate/dimethyl carbonate (EC/DMC).

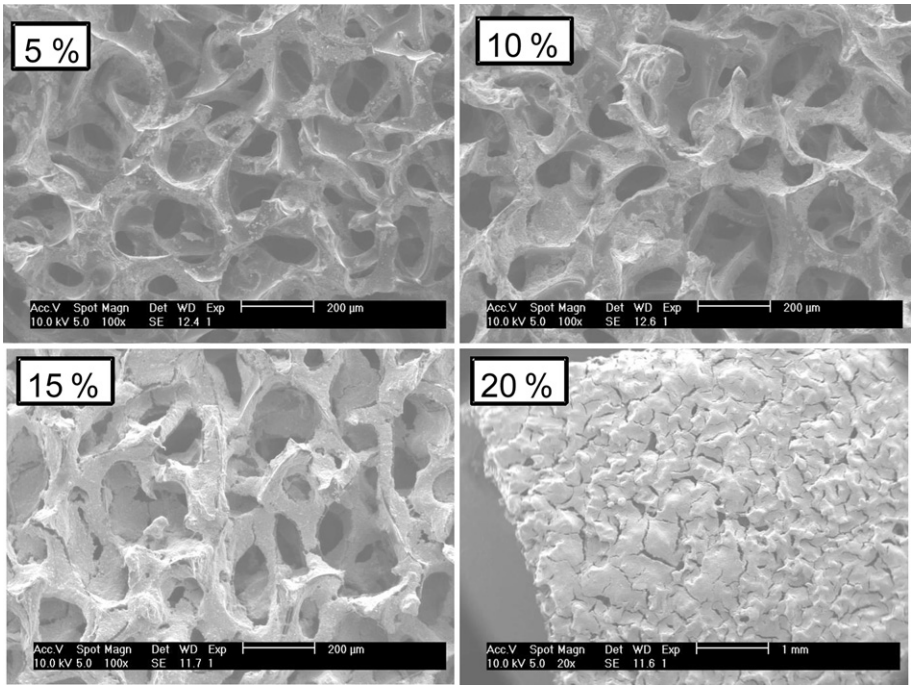

Fig. 4. SEM images of reticulated vitreous carbon substrates coated with a layer from $LiFePO_4$ inks with 5, 10, 15 and 20 wt. % solids as indicated in the images.

3. Results and discussion

3.1. Initial development of the dip–spin coating method

Initial experiments focused on the development of the dip–spin coating method based on the following example. A 10 × 5 × 1 mm sample of RVC foam and a 10 wt. % $LiFePO_4$ ink were prepared as described in the Experimental Section. The end (bottom 1 mm) portion of foam was immersed slowly into the ink to allow the air to escape and prevent the formation of air pockets; during this time the ink was seen to fill the whole 10 mm of the foam via capillary action within a few seconds. The ink soaked foam was then attached to the spinning apparatus, shown schematically in Fig. 1, and spun for 30 s in an attempt to remove the ink from the center of the pores while allowing a coating to remain on the walls and dry *in-situ*. Repeating the process with different spinning rates showed that uniform coatings over the entire internal surface of the samples were produced when the highest spinning rates were used (2000 rpm at a 3 cm radius), whereas some agglomeration and pore blocking occurred at lower rates.

These experiments showed that it was possible to deposit a relatively even coating of $LiFePO_4$ composite electrode ink over the internal structure of the RVC electrodes. A further series of experiments investigated the effect of the weight percentage of solid within the ink and the numbers of dip–spin coating cycles. Finally the same method was used to deposit uniform coatings of $LiMn_2O_4$ and TiO_2 composite inks on 3D substrates.

3.2. Optimization of the ink

The consistency of the ink was found to be extremely important in achieving a good homogeneous coating throughout the RVC substrate. $LiFePO_4$ inks were prepared with 5, 10, 15 and 20 wt. % of solid material as described in the experimental section. Compared with the initially smooth struts and wide pores of the bare foams in Fig. 3, the SEM images in Fig. 4 show the coatings as light areas of particulate. The deposit shows no obvious morphological distinction between the $LiFePO_4$ particles and the carbon or polymer binder at the resolution used and there was no tendency to form large agglomerates. To observe the presence and distribution of $LiFePO_4$ in the composite, energy dispersive X-ray (EDX) spectra were recorded of selected areas of the struts. These showed intense peaks confirming the predominance of Fe, P, C and O in the coating. Li was undetected due to its low atomic number but its presence was inferred from the detection of Fe and P.

Fig. 4 gives a qualitative impression of an increase in the loading of $LiFePO_4$ without pore blocking on increasing the amount of solids in the ink up to 15 wt. %; however, when 20 wt. % inks were used all pores appeared blocked. Subsequently, mixtures prepared with 5 and 10 wt. % solid component were considered as the most suitable for fabrication of 3D dip–spin coated composite/RVC electrodes.

To take full advantage of the enhanced surface area afforded by the RVC, the cathode coating should penetrate to the very center of the foam. Such penetration is confirmed in Fig. 5, which shows

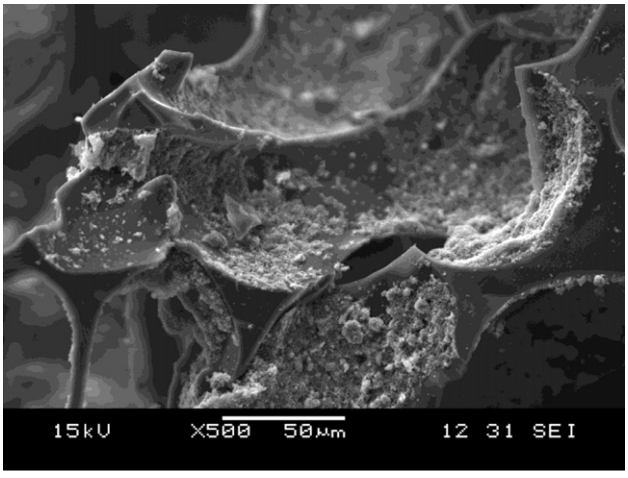

Fig. 5. An SEM image of the $LiFePO_4$ coverage in the center of the foam.

a cross section cut from the center of the sample. Occasionally, bare foam can be seen at asperities; however, small gaps in a macroscopically uniform electrode layer should not result in a problem, by contrast with a separator layer in which pinholes cause short circuits that would prevent operation of the battery.

3.3. Electrochemical characterization

The $LiFePO_4$/RVC electrodes were tested galvanostatically in a "semi 3D" condition where the foam cathode was cycled in liquid electrolyte vs. a planar lithium anode. Fig. 6a shows that the expected plateau at around 3.4 V vs. Li for $LiFePO_4$ associated with the 2 phase insertion of Li^+ into $FePO_4$ was observed and gives a quantitative assessment of the effect of increasing the solid content of the ink from 5 to 10 wt. %. A capacity per footprint area Q_f, of ~325 μA h cm^{-2} was achieved with a single dip–spin coating deposition in the 10 wt. % ink case. In the case of the electrode prepared using 10 wt. % ink we also show the cyclabilty in Fig. 6b while testing the electrode with a number of different rates. The graph shows that there is very little degradation per cycle with 98% capacity retention seen at a rate of 0.2 C after 43 cycles at various rates. This strongly suggests that both the electrode material and the adhesion of the films to the substrate is stable during electrochemical cycling. The electrodes prepared using a higher percentage ink (15 wt. % ink) yielded higher capacities (not shown) at low rates of discharge, however, those electrodes were deemed unsuitable for use in the full 3D microbattery configuration because of potential pore blocking issues. Therefore, to increase the footprint area capacity further a sequential spin coating process was investigated to increase the composite thickness and capacity as described below.

The maximum capacity per mass of $LiFePO_4$ at a low rate, Q_m^o, has been estimated as close to the normal practical capacity of 150 mA h g^{-1} ± 20%, with the large error estimate being due to difficulties in weighing small coating masses in the fragile samples. Accordingly, the volume of composite electrode material per footprint area can be calculated from Equation (1) below, using a typical value of about 1.2 g cm^{-3} for the composite density, ρ, (mass of $LiFePO_4$ per volume of composite) obtained in our previous studies of composite electrodes of similar composition [10]. This volume/area ratio can be regarded as the thickness L, of a planar composite electrode with the same capacity per footprint area.

The composite electrode volume per footprint area, expressed as a thickness can be expressed as:

$$L = \frac{Q_f}{Q_m^o \times \rho} = \frac{0.325\ \text{mAh cm}^{-2}}{150\ \text{mAh g}^{-1} \times 1.2\ \text{g cm}^{-3}} = 18\ \mu\text{m} \qquad (1)$$

Combining this value with the previous estimate of an area enhancement factor of approximately 30 due the 3D architecture of the foam, we obtain an average coating thickness as 0.6 μm, which is lower than that estimated (2–3 μm) from the SEM images. The lower value is partly due to some non-uniformity of the coating but also it is likely that this technique results in a less dense coating than that achieved in our previous work in which the electrodes were compressed using a rolling mill.

3.4. Increased loading coatings by sequential spinning

To increase the specific capacity per footprint area of the $LiFePO_4$/RVC electrodes whilst maintaining good porosity, the substrates were subjected to several dip–spin coating cycles. A 10 wt. % ink was selected for this study as it provided good coverage whilst maintaining porosity within the sample. SEM images of the $LiFePO_4$/RVC electrodes after 1, 2, 3 and 4 dip–spin coating cycles are shown in Fig. 7 where the $LiFePO_4$ composite deposition is clearly visible on the surface of the RVC substrate in each case. Surprisingly, evidence of increased $LiFePO_4$ composite film thickness is not clearly shown.

Galvanostatic cycling of the $LiFePO_4$/RVC electrodes in liquid electrolyte vs. a planar lithium anode resulted in the discharge profiles shown in Fig. 8a, where we can now see the capacity clearly increasing with increasing number of dip–spin coating cycles to give up to 1500 μA h cm^{-2}, equivalent to a planar electrode thickness of 80 μm according to Equation (1) and similar to the thickness of the electrode of commercial Li-ion cells. The linearity of the relationship between area specific discharge capacity and dip–spin coating cycles, shown in Fig. 8b, confirms that a new coat was applied each time without significantly dissolving the underlying layers, as had been a previous concern. The linear increase capacity does not, however, demonstrate a linear increase in the overall thickness, and given the lack of evidence of thickness increase in the SEM images, it is suspected that it is the overall density that increases with sequential dip–spin coating cycles by filling the voids in previously deposited layers. This interpretation

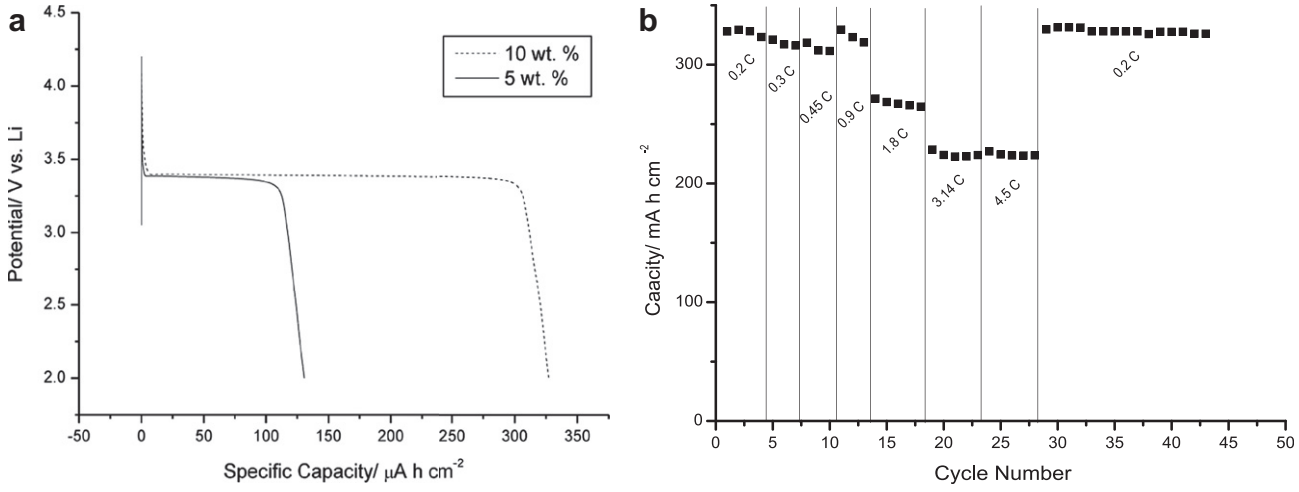

Fig. 6. a)Potential vs. capacity plot of the charge and discharge at ~C/2 for the $LiFePO_4$ composite coated RVC foams. (b) The cyclability of the RVC foam coated a $LiFePO_4$ electrode using the ink containing 10 wt. % solids.

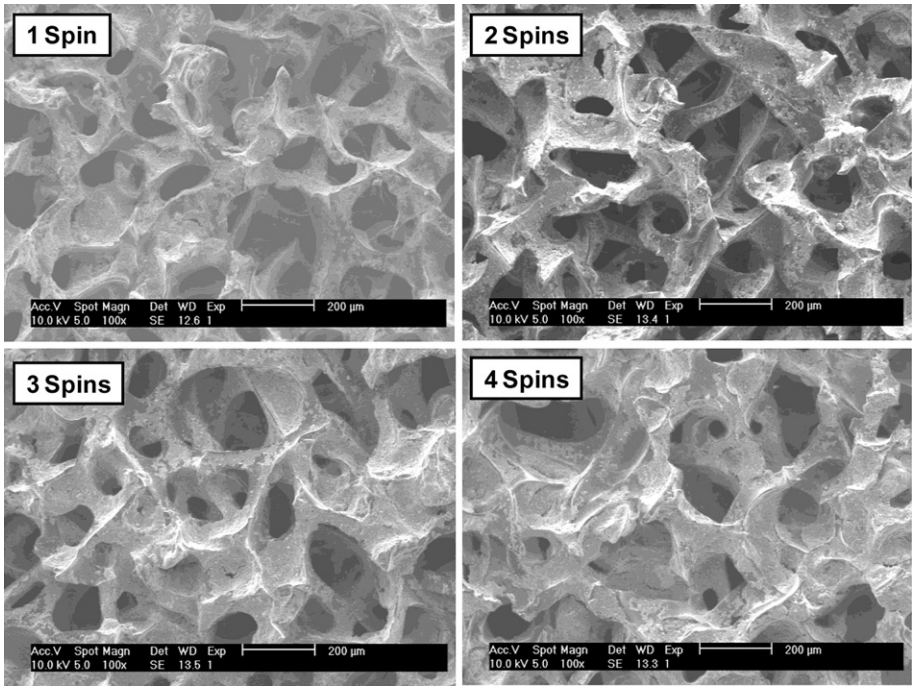

Fig. 7. SEM images of reticulated vitreous carbon substrates coated in $LiFePO_4$ from an ink with 10 wt. % solids. The foams were coated by 1, 2, 3 and 4 dip–spin coating cycles as indicated in the images.

is supported by applying Equation (1) and dividing by the enhancement factor as before to calculate an average strut coating thickness of 2.8 μm after 4 dip–spin coating cycles. The similarity of this result to what is observed in the SEM images indicates that the density approaches the 1.2 g cm^{-3} obtained in our previous work.

By comparing the average strut coating thickness estimated above with an average pore diameter of more than 100 μm it can be seen that the macrostructure of the $LiFePO_4$/RVC electrodes remained relatively porous. This porosity should allow enough room to accommodate the electrolyte, anode and current collector layers necessary to complete the full 3D microbattery.

The capacity vs. rate performance of the dip–spin coated $LiFePO_4$/RVC electrodes vs. increasing numbers of dip–spin coating cycles is shown in Fig. 9a. In all cases the discharge capacity tended toward a maximum at low C-rate (below C/0.9, C/1.2 and C/1.5 for the 4, 3 and 2 cycle samples respectively) corresponding to the fully discharged condition. The materials exhibit good high discharge rate performance and all electrodes showed good capacity retention at high rate; in particular, the RVC electrode coated with 3 layers of dip–spin coated $LiFePO_4$ achieved a 50% (500 μA h cm^{-2}) degree of discharge at ~25 C. For comparison, a planar electrode of similar capacity per footprint with a thickness of approximately 60 μm was prepared and tested. Fig. 9b shows the rate performance

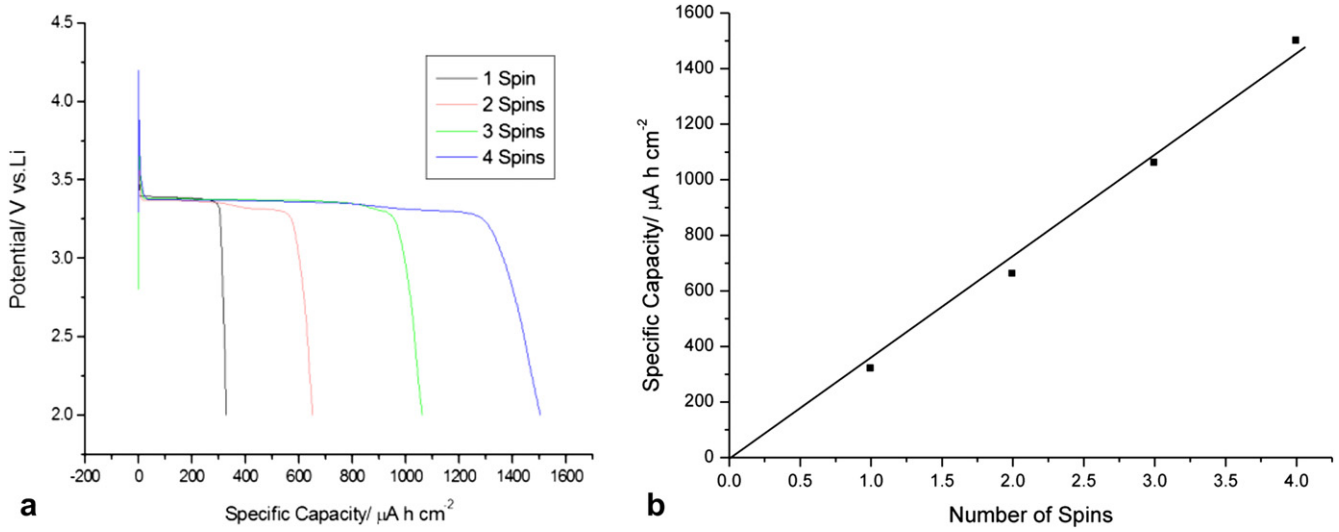

Fig. 8. a) First discharge curves for the foams coated 1, 2, 3 and 4 times with the 10 wt. % ink at discharge rate ~C/2 (b) the specific capacity at C/2 vs. the number of dip–spin coating steps.

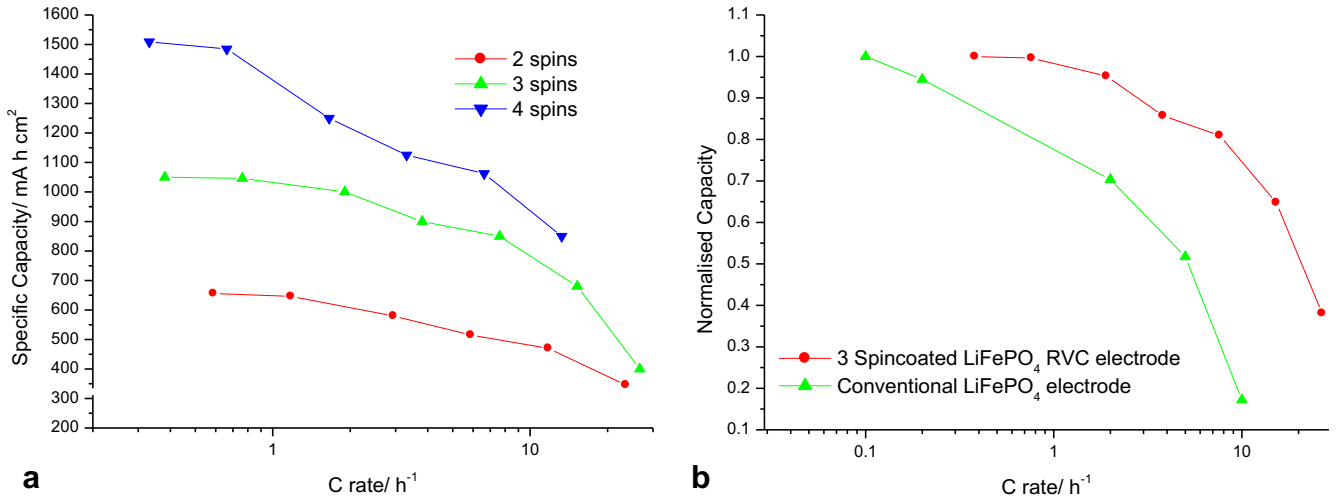

Fig. 9. (a) Rate performance summary of foams coated using dip–spin coating with 2, 3 and 4 layers of cathode. (b) Rate performance of 3 dip–spin coated electrode (slow rate capacity 1050 mAh cm^{-2}) compared to a conventional $LiFePO_4$ electrode (slow rate capacity 1150 mA h cm^{-2}). Capacities were normalized to slow rate capacity to highlight rate performance.

of this electrode compared to that of the 3 cycle dip–spin coated $LiFePO_4$/RVC electrode. We observe a significantly enhanced rate capability for the RVC electrode; the rate at which 50% capacity retention could be achieved in the conventional electrode was only ~5 C compared with the ~25 C for our $LiFePO_4$/RVC electrode.

Fig. 9 shows that extremely good rate performance was observed in all cases. However, the reduction in capacity is more rapid in the foams which have received a higher number of dip–spin coating cycles. At a rate of 10 C the retention of the 1 C capacity was 80, 75 and 60% for the 2, 3 and 4 spin coated electrodes respectively. This is consistent with the increase in mass loading, as observed in several previous studies which highlight high rate performances obtained by dilution of the active mass or decreasing the electrode thickness [10].

In Table 1 we compare the 3 and 4 cycle dip–spin coated $LiFePO_4$ electrodes with several topical examples found within the literature. The data shows that our electrode structures have competitive capacities per footprint areas which can be easily increased by further dip–spin coating steps. The rate capability of the material also compares extremely well with the literature examples shown. The work of Shaijumon et al. represents perhaps the highest rate capability where Ni pillars coated in $LiCoO_2$ retained up to 68% of the low rate capacity at ~7 C [22]. This highlights the extremely good performance seen in our material where 50% of the slow rate capacity was retained at a rate of 25 C. The electrochemical coatings of CuS and MnO_2 shown compare favorably in terms of capacity per footprint area, however, the rate performance is somewhat limited which we believe is a result of the lack of electronic conduction paths and long ionic diffusion lengths. This problem is alleviated in the layer formed using dip–spin coating which contains active material particles of optimal size for good ionic diffusion and electronic additive in the form of carbon black.

3.5. $LiMn_2O_4$ and TiO_2 coatings onto the RVC foam

The above results have demonstrated the viability of dip–spin coating as a method for depositing uniform films of $LiFePO_4$ onto 3D RVC electrodes. To demonstrate the versatility of the dip–spin coating approach, films of $LiMn_2O_4$ and TiO_2 were deposited onto the RVC substrates. The dip–spin coating was performed using the same technique as used to fabricate the $LiFePO_4$/RVC electrodes. Fig. 10 shows a uniform coating of particulate deposit on the RVC substrate from a 10 wt. % ink (similar to that seen with the $LiFePO_4$ electrodes). However, in comparison with the dip–spin coated $LiFePO_4$ films, larger particles can be clearly distinguished as embedded in the composite layer (particularly obvious in the high magnification image). The size and shape of these particles is consistent with the presence of $LiMn_2O_4$, which we have observed in the absence of any carbon or binder. The presence of $LiMn_2O_4$ was also confirmed using EDX measurements. Importantly these particles appear to be evenly distributed throughout the composite electrode.

Inks containing anatase TiO_2 nanoparticles were also applied to the substrate via dip–spin coating onto 3D RVC substrates, the resulting deposits are shown in Fig. 10. As with the previously deposited materials an evenly distributed composite electrode film was observed. However, due to the small size of the particles (~12 nm, BET) the morphological difference between the TiO_2 and the conductive carbon additive was not easily resolved. The presence of TiO_2 was also confirmed using EDX measurements.

Table 1
Comparison of the performance of the electrodes discussed in this work with other topical literature examples. The material presented here is highlighted in the shaded rows.

Material	Ref	Slow Rate Capacity/μA h cm^{-2}		High Rate Capacity/μA h cm^{-2}	
		Rate	Capacity	Rate	Capacity
Spin dried LFP/RVC (3 coats)	This work	~C/3	~1000	~25C	~500
Spin dried LFP/RVC (4 coats)	This work	~C/4	~1500	~17C	~849
Electrodeposited MnO_2/RVC	[14]	~C/20	~3000	2C	~150
Electrodeposited CuS/silicon microchannels	[12]	~C/8	~1100	~2C	~500
Electrophoretically deposited $LiFePO_4$/silicon microchannels	[13]	~C/50	~2300	N/A	N/A
Spray coated $LiCoO_2$/Aluminum pillars	[22]	~C/10	~125	~7C	~85

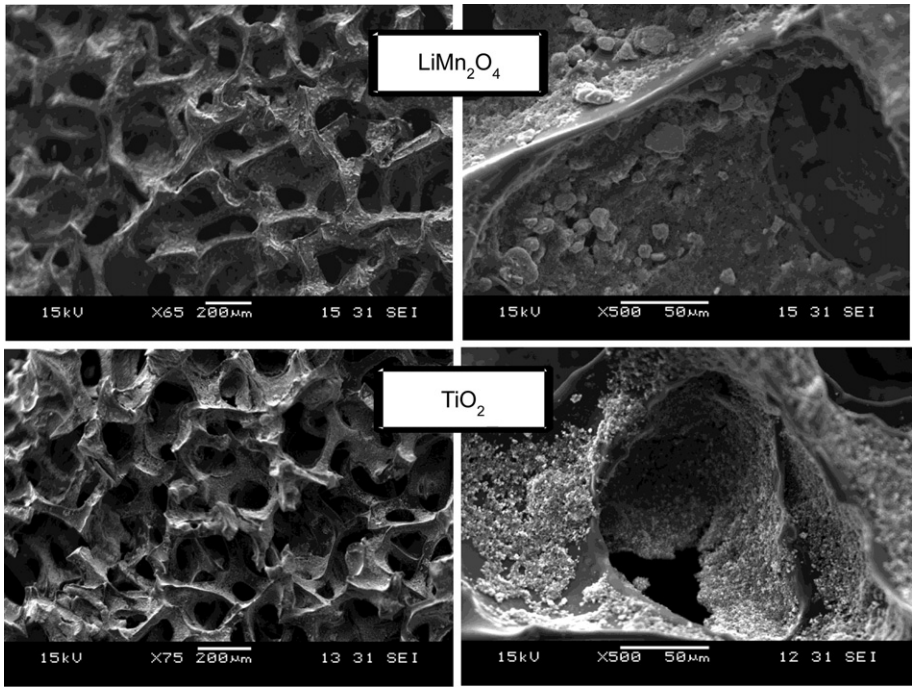

Fig. 10. SEM images of reticulated vitreous carbon substrates coated in $LiMn_2O_4$ and TiO_2. The images on the left side are taken at 75 times magnification and on the right 500 times magnification.

The successful deposition of both $LiMn_2O_4$ and TiO_2 onto high surface area 3D substrates illustrates that the technique of dip–spin coating can be readily adapted for the conformal deposition of any material that can be made in to a composite electrode ink. To confirm the resulting $LiMn_2O_4$ and TiO_2/RVC electrodes were electrochemically active they were cycled galvanostatically in liquid electrolyte vs. a planar lithium anode.

The resulting first discharge at C/10 for both electrodes is shown in Fig. 11. The discharges occurred over the characteristic potential ranges for both materials as reported in the literature. Discharge capacities of 900 and 1600 μA h cm^{-2} were observed for the $LiMn_2O_4$ and TiO_2 foams respectively. The capacity of the TiO_2/RVC electrode was 1.8 times that of the $LiMn_2O_4$ sample, roughly corresponding to the ratio in practical capacities of the two materials (~110 and ~200 mA h g^{-1} for $LiMn_2O_4$ [18] and TiO_2 [21] respectively). No obvious corrosion currents were seen from the RVC substrates at these more extreme potential ranges.

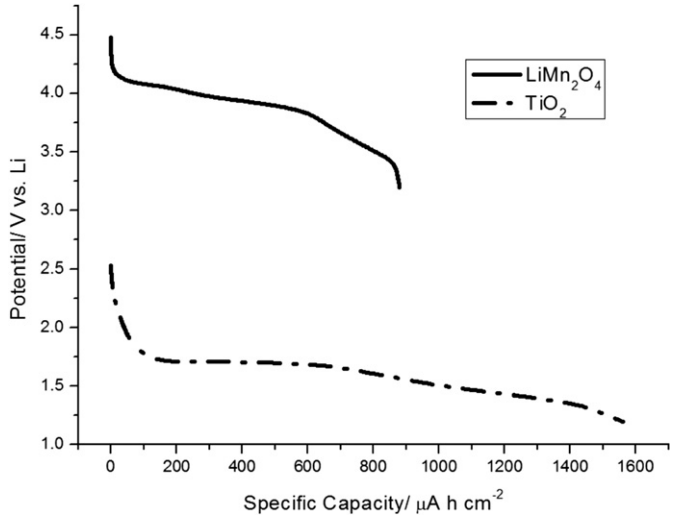

Fig. 11. First discharge voltage profiles for RVC foams coated in $LiMn_2O_4$ and TiO_2 prepared from 2 dip–spin coating steps using 10 wt. % inks at ~C/5 discharge.

Although the relative performance of $LiMn_2O_4$ and TiO_2 compared well with the $LiFePO_4$ samples, weighing difficulties again caused large errors in the estimation of the amount of active material, and in subsequent estimations of the gravimetric specific capacity and porosity which are important in estimating how close the state of the art is to the theoretical maximum. For this reason, thermogravimetric analysis (see supplementary information) was used to quantify the mass loading of $LiMn_2O_4$ achieved in the 2 spin sample as approximately 6.34 mg of $LiMn_2O_4$ per cm^2 of footprint. Fig. S1 (included as supplementary information) also shows TGA results of mass loadings of $LiMn_2O_4$ as a function of the number of dip–spin coating steps. The results indicate a linear relationship between the number of dip–spin coating steps and the mass loading. Using the 2-spin result in combination with the capacities per footprint quoted above, the gravimetric capacity of the $LiMn_2O_4$/RVC electrode was calculated as 134 mA h g^{-1}, close to the theoretical capacity (148 mA h g^{-1}) and slightly higher than the typical capacities seen when using conventional electrode preparations (110–120 mA h g^{-1}). This result indicates that the RVC composite electrode architecture allowed for the complete utilization of the available capacity. This important results suggests that all the active material within the dip–spin coated electrode is electronically wired to the RVC current collector and therefore electrochemically active.

3.6. Advantages of the dip–spin coating approach

The dip–spin coating approach for the fabrication of 3D microbattery electrodes outlined in this paper has several important advantages over alternative fabrication methods.

The process is relatively cheap and simple employing commercially available substrates and uncomplicated apparatus.

This is a particular benefit when compared to the specialized equipment and expensive time consuming fabrication techniques utilized in photolithographic or complicated etching procedures common within other microbattery approaches.

The versatility of the dip–spin coating technique allows for the deposition of any active material, so long as it can be made into a composite electrode ink (this is of particular note when this technique is compared to electrochemical deposition). This allows the deposition of well characterized and understood conventional lithium battery materials and can be particularly advantageous in the deposition of lithium containing electrodes.

The majority of literature examples focus on the deposition of both cathode and anode materials without the inclusion of lithium ions which will limit the construction of full 3D microbatteries where the lithium will need to be present in one electrode (notable exceptions are the work of Shaijumon et al. [22] and Mazor et al. [13]). In principle, the dip–spin coating method can be used to deposit all layers of the electrode/electrolyte/electrode cell structure on a 3D substrate. This is of particular note for the application of the second electrode which has been notoriously difficult using electrodeposition.

The dip–spin coated layers also include conductive additive and binders which allow for normal operation of these battery materials (again, another significant advantage over electrochemical deposition where typically only the active material is deposited). This also means that the coatings are porous and allow for good ionic diffusion of the lithium salt through the cathode layer.

Finally, application of the 3D concept to larger batteries is an attractive prospect for high rate capability and a feasible prospect given adequate scalability of the deposition techniques. Therefore it is a significant result of this work that the dip–spin coating process has been applied successfully to 3D structures that are relatively large compared to the 3D microbatteries frequently discussed in the literature applications.

It is perhaps worth considering the potential drawbacks of this technique and areas that require further investigation. One potential limitation of this technique may be in targeted deposition, where layers need to be deposited onto a device containing many different integrated components. This may be possible with careful masking but may be impractical to implement. A second drawback is the level of waste material which is spun onto the walls of the coating chamber during the coating procedure; however, we envisage that much waste material could be recovered and used for further coatings.

Finally, the effectiveness of the dip–spin coating technique when using substrates with much smaller pore sizes, where blocking of the smaller pores will be more difficult to avoid, remains to be seen. In these situations electrochemical coating techniques (which have been demonstrated on pore sizes in the $<$10 nm range) may be more appropriate.

4. Conclusion

To the best of our knowledge we have demonstrated the first example of a 3D structured current collector being coated with a conventional composite electrode containing active material, conductive additive and binder. The important inclusion of these components means that the active material performance will not be restricted by electronic or ionic conductivity problems that have been previously observed [14], this was achieved by employing a novel dip–spin coating technique. This method produced uniform coatings with no observable pore blocking and room for the addition of subsequent layers of electrolyte, second electrode and current collector required to fabricate a full 3D microbattery. This highly economical approach was easily achieved with a simple setup that did not require specialist equipment or a complicated fabrication process. The mass loading of the active materials on the 3D substrate was easily controlled by manipulating the weight percentage of solids in the ink and by varying the number of dip–spin coating cycles. It is envisaged that this will lead to an effective method of balancing the capacity of the cathode and anode in a full 3D microbattery. This approach has been demonstrated for several different electrode materials.

Electrodes prepared using the dip–spin coating method were tested electrochemically and extremely high footprint capacities were achieved. The $LiFePO_4$/RVC electrode fabricated using 3 dip–spin coating cycles and a 10 wt. % solids ink achieved an area specific capacity of 1000 μA h cm^{-2} at a 1 C discharge rate and 500 μA h cm^{-2} at a discharge rate of 25 C. Capacities up to two or three times higher may be expected on further optimization to increase the film densities.

High footprint-specific capacities were also achieved for $LiMn_2O_4$ and TiO_2 composite/RVC electrodes. The adaptation of the dip–spin coating process to a number of electrode materials demonstrated the versatility of the technique and proved that it was possible to form dip–spin coatings using inks containing active materials with a variety of particle sizes.

Acknowledgments

This work was supported by the EC FP7 Superlion project; we would also like to thank Stéven Renault at Uppsala University for assistance the TGA measurement.

Appendix A. Supplementary data

Supplementary data related to this article can be found at http://dx.doi.org/10.1016/j.jpowsour.2012.09.103.

References

[1] M. Roberts, P. Johns, J. Owen, D. Brandell, K. Edstrom, G. El Enany, C. Guery, D. Golodnitsky, M. Lacey, C. Lecoeur, H. Mazor, E. Peled, E. Perre, M.M. Shaijumon, P. Simon, P.-L. Taberna, Journal of Materials Chemistry 21 (2011) 9876.
[2] D. Golodnitsky, V. Yufit, M. Nathan, I. Shechtman, T. Ripenbein, E. Strauss, S. Menkin, E. Peled, Journal of Power Sources 153 (2006) 281–287.
[3] D. Golodnitsky, M. Nathan, V. Yufit, E. Strauss, K. Freedman, L. Burstein, a. Gladkich, E. Peled, Solid State Ionics 177 (2006) 2811–2819.
[4] J.W. Long, K.E. Swider-Lyons, R.M. Stroud, D.R. Rolison, Electrochemical and Solid-State Letters 3 (2000) 453.
[5] H.-S. Min, B.Y. Park, L. Taherabadi, C. Wang, Y. Yeh, R. Zaouk, M.J. Madou, B. Dunn, Journal of Power Sources 178 (2008) 795–800.
[6] R.W. Hart, H.S. White, B. Dunn, D.R. Rolison, Electrochemistry Communications 5 (2003) 120–123.
[7] G. El-Enany, M.J. Lacey, P.a. Johns, J.R. Owen, Electrochemistry Communications 11 (2009) 2320–2323.
[8] J.F.M. Oudenhoven, L. Baggetto, P.H.L. Notten, Advanced Energy Materials 1 (1) (2010) 10–33.
[9] J.W. Long, B. Dunn, D.R. Rolison, H.S. White, Chemical Reviews 104 (2004) 4463–4492.
[10] P. Johns, M. Roberts, Y. Wakizaka, J.H. Sanders, J. Owen, Electrochemistry Communications 11 (2009) 2089–2092.
[11] M. Nathan, D. Golodnitsky, V. Yufit, E. Strauss, T. Ripenbein, I. Shechtman, S. Menkin, E. Peled, Journal of Microelectromechanical Systems 14 (2005) 879–885.
[12] H. Mazor, D. Golodnitsky, L. Burstein, E. Peled, Electrochemical and Solid-State Letters 12 (2009) 232–235.
[13] H. Mazor, D. Golodnitsky, L. Burstein, A. Gladkich, E. Peled, Journal of Power Sources 198 (2012) 264–272.
[14] P. Johns, M. Roberts, J. Owen, Journal of Materials Chemistry 21 (2011) 10153.
[15] A.K. Padhi, K.S. Nanjundaswamy, J.B. Goodenough, Journal of the Electrochemical Society 144 (1997) 1188–1194.
[16] A.K. Padhi, K.S. Nanjundaswamy, C. Masquelier, S. Okada, J.B. Goodenough, Journal of the Electrochemical Society 144 (1997) 1609–1613.
[17] M.M. Thackeray, Progress in Solid State Chemistry 25 (1997) 1–71.
[18] M.M. Thackeray, P.J. Johnson, L.A. de Picciotto, P.G. Bruce, J.B. Goodenough, Materials Research Bulletin 19 (1984) 179–187.

[19] M.M. Thackeray, A.D. Kock, M.H. Rossouw, D. Liles, R. Bittihn, D. Hoge, Journal of The Electrochemical Society 139 (1992) 363.
[20] K.H. Reiman, K.M. Brace, T.J. Gordon-Smith, I. Nandhakumar, G.S. Attard, J.R. Owen, Electrochemistry Communications 8 (2006) 517–522.
[21] A.R. Armstrong, G. Armstrong, J. Canales, R. Garcia, P.G. Bruce, Advanced Materials 17 (2005) 862–865.
[22] M.M. Shaijumon, E. Perre, B. Daffos, P. Taberna, J.-M. Tarascon, P. Simon, Advanced Materials 22 (2010) 4978–4981.